IEEE Access
Multidisciplinary | Rapid Review | Open Access Journal

Received 31 May 2022, accepted 29 June 2022, date of publication 4 July 2022, date of current version 15 July 2022.

Digital Object Identifier 10.1109/ACCESS.2022.3188281

RESEARCH ARTICLE

A Dynamic Bayesian Network Model for Real-Time Risk Propagation of Secondary Rear-End Collision Accident Using Driving Risk Field

XIANMIN SONG, YAQIAN SUN, AND PENGFEI TAO
School of Transportation, Jilin University, Changchun 130022, China

Corresponding author: Pengfei Tao (taopengfei@jlu.edu.cn)

This work was supported in part by the National Key Research and Development Program of China under Grant 2019YFB1600500, and in part by the Jilin Province Natural Science Foundation of China under Grant 20190201107JC.

ABSTRACT In order to take more active measures to prevent and control secondary accidents, it is necessary to describe risk propagation process after the accident. To this end, this paper deeply analyzed the risk propagation mechanism between vehicles and proposed a novel secondary rear-end collision accident risk propagation model, which could real-time evaluate vehicle rear-end collision risk. The research scene of the paper is a single-lane road rear-end collision scene, so a driving risk field model suitable for this scene is first established. Based on this, the vehicle operation interaction risk field force is calculated. Then, the risk field force is converted into risk probability through the hyperbolic tangent function, and the vehicle operation interaction risk model is obtained. In addition, a risk propagation framework based on dynamic Bayesian network is constructed to describe the propagation process of rear-end collision risk from the accident vehicle to following vehicles. Finally, according to the probabilistic reasoning process of the framework, combined with the accident vehicle risk, a secondary rear-end collision accident risk propagation model is established. Simulation experiments show that the paper model can describe the evolution trend of rear-end risk and the risk assessment results are more accurate. And after the accident, the rear-end collision risk propagation speed will increase with the increase of traffic flow, and the number of secondary rear-end vehicles will also increase with the increase of traffic speed. These conclusions are of great significance in formulating vehicle anti-collision strategies and deploying risk management and control facilities.

INDEX TERMS Secondary rear-end collision, risk propagation, driving risk field, dynamic Bayesian network.

I. INTRODUCTION

Traffic flow status is affected by drivers, vehicles, road, environment, and traffic management. Driver and vehicle are dynamic factors, which determine the safety of road system. When the traffic flow is running on the road, vehicle spacing and speed are not the same, but the system is in the state of balance. When a traffic accident breaks out, the balance of the system is broken by this random factor. Following vehicles' speed will have different reaction. The uncoordinated reaction of many vehicles will lead to secondary accidents. According to the five-year traffic accident data statistics of Sanmenxia Expressway in China, a total of 1640 accidents occurred in this road, resulting in 96 deaths and 245 injuries, of which the secondary accidents accounted for 57.3%, 54.2% and 67.3% respectively, and the degree of harm far exceeds that of the first accident. Therefore, the real-time assessment of vehicle risk is the theoretical basis for the prevention of secondary accidents.

Vehicle operation risk assessment methods mainly include deterministic method and probabilistic method [1], [2]. Deterministic method usually used the conflict indicators of time, distance, and deceleration to distinguish whether the vehicle collision occur. Many scholars used the single conflict

The associate editor coordinating the review of this manuscript and approving it for publication was Xiangxue Li.

indicator to evaluate vehicle collision risk [3]–[6]. These researches showed that using different indicator has different evaluation result [7]. Therefore, in order to improve the collision discrimination effect, some scholars used multiple indicators to distinguish. For example, Christos combined TTC and DRAC to distinguish vehicle collision [8]. In previous studies, conflict indicators were often used to assess historical vehicle collision risk, and only in a few studies were used to assess real-time vehicle collision risk. Ma and Xie predicted vehicle trajectory and used PET & TTC to estimate the real-time vehicle collision risk [9], [10]. With the rise of data-driven algorithms, some studies used the machine learning algorithm to assess vehicle risk [10], [12], [13]. Chen applied fault tree analysis and k-Means clustering algorithm to determine risk labels of prior trajectories based on Crash Potential Index, and used random forest to predict lane change risk [14]. Shi also used Fuzzy C-means clustering algorithm and XGBoost classifier combined with TTC and DRAC to realize vehicle trajectory marking and driving risk prediction [15]. To sum up, although many studies have proved that the conflict index can effectively estimate the collision risk of vehicles, the conflict index model focuses too much on the operating parameters of vehicles and lacks the consideration of risk factors such as driver operation, road design and weather conditions [16]. And binary evaluation characteristics of the existing conflict indicators will lead to the instability of continuous evaluation results of vehicle risk [17], so the robustness of deterministic method is poor.

Probabilistic method is not a binary evaluation method to judge whether a vehicle collision will happen or not [1], [2]. This method generally uses various risk factors to construct the risk index to reflect the vehicle risk probability. Ma and Yan used data such as driver's operation, eye movement behavior, driver experience and vehicle performance to quantify the driving risk probability index [18]–[20]. Ding established a risk field combining vehicle speed and relative distance, and described the current vehicle risk through the risk field force index [21]. In order to further describe the impact of driver behavior characteristics, road conditions and traffic environment on vehicle safety, Wang linked the risk field with the electric field and proposed the circular structure risk field model coupling human, vehicle, and road for the first time, which provided a new research idea for vehicle risk assessment [22]–[24]. In order to quantitatively evaluate driving risk, the scholar transformed risk field force into safety potential energy by integral method, and thus proposed the DSI safety driving index [25]. Li thought that the risk field without acceleration parameters could not express the change of vehicle movement trend, and the circular structure could not express the difference of field intensity distribution under the influence of speed. He designed the elliptic structure risk field combined with acceleration parameters, and thus proposed the PFI traffic risk index and established the vehicle collision early warning framework [26]–[28]. Now, the application of risk field theory has become a powerful means of vehicle risk assessment [29]. In addition, in order to make the risk assessment results predictable, some scholars combined the vehicle motion prediction model and intention recognition model to estimate future vehicle risk [30], [31]. Generally speaking, probabilistic method has greater performance in describing the uncertainty of vehicle risk.

Although many scholars have achieved excellent research results in vehicle risk assessment, there is still a problem. At present, most of the risk assessment methods for rear-end collisions focus on considering the operating parameters of vehicles, ignoring the effect of the risk of the leading vehicle on the rear-end collision of the following vehicle, that is, the mechanism of risk transmission between vehicles is unclear. Based on this, in the process of studying the risk propagation of secondary rear-end collisions, the paper adopts the probabilistic risk assessment method based on risk field, and establishes a secondary rear-end collision accident risk propagation model through dynamic Bayesian network combining the operating parameters of two vehicles and the risk of the leading vehicle. In order to achieve a preliminary study on the risk propagation characteristics of rear-end collision accidents.

The main contributions of this paper can be summarized as follows. (1) The paper deeply analyzes the risk propagation mechanism between vehicles, and puts forward a risk assessment method of secondary rear-end collision accident combined with driving risk field and dynamic Bayesian network(DBN). (2) The paper establishes a driving risk field model suitable for single-lane road rear-end collision scenarios, which emphasizes the adjustment of speed to field intensity distribution. (3) The paper constructs an operation interaction risk model with risk field force as parameter and proposes an accident vehicle risk model based on the principle of risk transfer. (4) The paper constructs a dynamic Bayesian network framework to describe risk propagation and establishes the secondary rear-end collision accident risk propagation model, which has the advantage of considering the leading vehicle risk. (5) The experiment proves the rationality of risk propagation model, and analyzes micro and macro propagation characteristics of risk with the change of traffic state.

The rest of the paper is arranged as follows. Section 2 analyzes risk transfer mechanism. Section 3 describes the construction process of secondary rear-end collision accident risk propagation model. Section 4 makes relevant experiments and analysis. section 5 summarizes the full text.

II. RISK TRANSFER MECHANISM ANALYSIS

As shown in Fig. 1, the following vehicle follows the leading vehicle on a single-lane road. When a rear-end collision accident occurs in front of two vehicles, the accident risk will spread backward. In order to avoid secondary rear-end collisions, the two vehicles will adjust their operating states. For the following vehicle, if it is adjusted incorrectly, it may hit the leading vehicle. If it is adjusted correctly but the leading vehicle is adjusted incorrectly, it may also hit the leading vehicle. Think about it another way. For the leading vehicle,

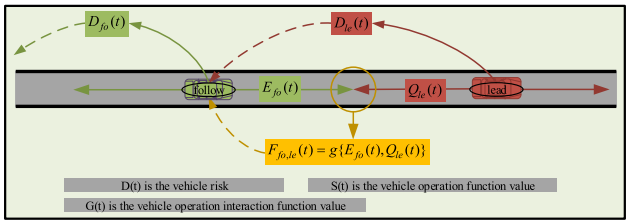

FIGURE 1. Risk transfer mechanism between vehicles.

it always has the risk of secondary rear-end collision and may have an accident at any time. Thus, its potential rear-end collision accident risk will invisibly increase the secondary rear-end collision accident risk of the following vehicle. Therefore, in essence, the secondary rear-end collision accident risk of the following vehicle should be closely related not only to the operation interaction risk of following & leading vehicle, but also to the risk propagation of the leading vehicle. This is the risk transmission process between vehicles. So, the secondary rear-end collision accident risk of the following vehicle can be expressed as $D_{fo}(t) = f\{F_{fo,le}(t), D_{le}(t)\}$.

The paper assumes that vehicle risk propagation on single-lane roads only exists between two adjacent vehicles. Considering that the occurrence of secondary rear-end collision accidents is the result of uncoordinated interaction among vehicles, it is very intuitive and visual to use the risk field force to describe vehicle operation interaction. And the risk assessment based on risk field can get real-time and continuous risk assessment results, which makes the risk assessment meaningful. In addition, considering that the total probability reasoning process of dynamic Bayesian network can effectively express vehicle risk transmission, and its conditional probability calculation principle can effectively describe vehicle operation interaction [32], [33]. Therefore, the paper finally puts forward a risk assessment method for secondary rear-end collision accident based on risk field theory and dynamic Bayesian network.

Based on this, the key to modeling the secondary rear-end collision accident risk propagation model is to calculate the operation state function values $Q_{le}(t)$ and $E_{fo}(t)$ of leading & following vehicle and describe their coupling relationship with the leading vehicle risk $D_{le}(t)$. Therefore, this paper first establishes a driving risk field model E, and uses the driving risk field intensity $E_{fo}(t)$ to describe the impact strength of the current operation of the following vehicle on the leading vehicle. Then an operation influence function Q is proposed, and the influence function value $Q_{le}(t)$ is used to describe the influence of the current operation of the leading vehicle on the rear-end collision of the following vehicle. Therefore, the operation interaction result $F_{fo}(t)$ of leading & following vehicle can be expressed as the function of $Q_{le}(t)$ and $E_{fo}(t)$. Finally, the paper uses the full probability inference process of dynamic Bayesian network to couple $F_{fo,le}(t)$ and $D_{le}(t)$ to obtain the secondary rear-end collision accident risk propagation model.

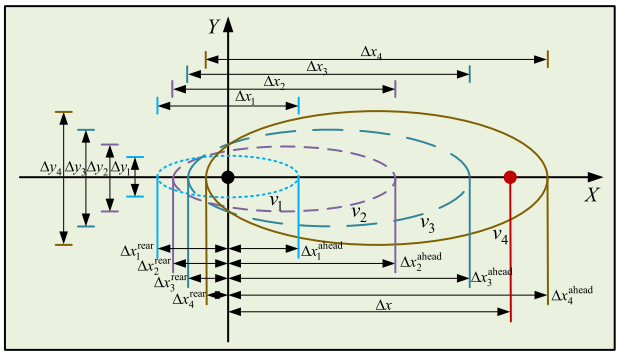

FIGURE 2. Change characteristic of effective influence range of driving risk field intensity.

III. MODEL CONSTRUCTION

This section constructs a driving risk field suitable for rear-end collision scenarios, and proposes a rear-end collision influence function of the leading vehicle, and transforms the risk field forces calculated by the two into the vehicle operation interaction risk. Then, a risk propagation framework based on dynamic Bayesian network is built to describe the propagation and influence process of the leading vehicle risk. Finally, we obtain the secondary rear-end collision accident risk propagation model.

A. CONSTRUCTION OF DRIVING RISK FIELD MODEL

1) MODELING IDEA

This paper studies the risk propagation of secondary rear-end collision accidents, so the established driving risk field should be suitable for vehicle rear-end collision scenarios. Because the speed of the following vehicle is too high and the driver's response of the following vehicle is not timely are the essential cause of the secondary rear-end collision accident, driving risk field E should be composed of vehicle kinetic energy field E_1 and driver behavior field E_2. The driving risk field intensity is defined as the impact strength of the vehicle on the surrounding space, which can reflect the severity of the rear-end collision to a certain extent. The paper screened out the main influencing factors of rear-end collisions and divided them into speed v, acceleration a, weight m, road environment factor γ and driver factor σ, which were used as the influencing factors of the risk field intensity. Thus, the driving risk field E can be describes by the parameters shown in (1).

$$E = \varphi(v, a, m, \gamma, \sigma) \tag{1}$$

This paper takes speed as the main parameter and other factors as auxiliary parameters to establish the driving risk field. For the same vehicle, the paper believes that when other factors remain unchanged, the change of vehicle speed will cause the change of the effective influence range of driving risk field intensity, including transverse range and longitudinal range. The specific change characteristic is shown in Fig. 2.

The black dot is the following vehicle position. The red dot is the leading vehicle position. The following vehicle

speed is $v_1 < v_2 < v_3 < v_4$. Under these four speeds, the maximum impact range of the following vehicle on the surrounding is shown by four different ellipses. This is also the biggest influence boundary of the driving risk field intensity. In the process of speed change, the change characteristic of transverse impact range is $\Delta x_1 < \Delta x_2 < \Delta x_3 < \Delta x_4$, the change characteristic of longitudinal impact range is $\Delta y_1 < \Delta y_2 < \Delta y_3 < \Delta y_4$, the change characteristic of rear impact range is $\Delta x_4^{\text{rear}} < \Delta x_3^{\text{rear}} < \Delta x_2^{\text{rear}} < \Delta x_1^{\text{rear}}$, the change characteristic of front impact range is $\Delta x_1^{\text{ahead}} < \Delta x_2^{\text{ahead}} < \Delta x_3^{\text{ahead}} < \Delta x_4^{\text{ahead}}$, and always keep $\Delta y < \Delta x$ and $\Delta x^{\text{rear}} \leq \Delta x^{\text{ahead}}$. The above is the paper's assumption that the shape of the driving risk field changes with the speed of the vehicle in the rear-end collision scenario. Δx is the distance between the leading vehicle and the following vehicle. Obviously, when the speed is v_4, $\Delta x < \Delta x_4^{\text{ahead}}$. This means that if the speed of the following vehicle is too high, the risk of rear-end collision will be greater. Based on the above analysis, as the components of the driving risk field, the field intensity variation law of the vehicle kinetic energy field E_1 and the driver behavior field E_2 should be consistent with the above assumptions.

2) DRIVING RISK FIELD MODEL

The vehicle kinetic energy field refers to the field formed by the vehicle as the main body and has nothing to do with the driver. Its field intensity should only be affected by vehicle speed v, acceleration a, weight m, road environment factor γ and adjustment coefficient λ, and the kinetic energy field E_1 can be expressed by the parameters shown in (2).

$$E_1 = \psi(v, a, m, \gamma, \lambda) \tag{2}$$

Since the basic distribution shape of the kinetic energy field is an ellipse, the paper uses the ellipse equation as the basic formula to model the kinetic energy field. Considering that the distribution shape of the kinetic energy field becomes more and more wide and long as the speed increases, the speed function is expressed as an exponential function $\varphi_1(v)$. As shown in (3). The coefficients κ and κ_1 can adjust the influence degree of speed on the ellipse shape.

$$\varphi_1(v) = (\kappa v)^{\kappa_1} \tag{3}$$

The horizontal and vertical ranges of the kinetic energy field intensity distribution are different. The speed functions $e^{\varphi_1(v)}$ and $\kappa_2 \cdot e^{\varphi_1(v)}$ are respectively introduced into the denominator of the elliptic equation to adjust the length of the long axis and the short axis, thereby controlling the variation of the kinetic energy field intensity distribution with the speed. Thus, the simple kinetic energy field model based on elliptic equation can be expressed as:

$$\left(\frac{|E_1| \cdot (x - x_0)}{e^{\varphi_1(v)}}\right)^2 + \left(\frac{|E_1| \cdot (y - y_0)}{\kappa_2 \cdot e^{\varphi_1(v)}}\right)^2 = 1 \tag{4}$$

Since the acceleration behavior will reduce the impact of the vehicle on the rear and the deceleration behavior will reduce the impact of the vehicle on the front, it is necessary to consider their weakening effect on the local field intensity. The paper uses the water drop line model to improve the kinetic energy field shape. The water drop line model with the vehicle as the center point and the acceleration and deceleration as the morphological adjustment parameters is shown in (5).

$$\left(\frac{x - x_0}{-a/|a|}\right)^2 + \left(\frac{y - y_0}{\sin(\theta/2)^{|a|}}\right)^2 = 1 \tag{5}$$

$|a|$ is the absolute value of the acceleration, and the item $-a/|a|$ can change the direction of water drop line and express the opposite weakening effect of acceleration and deceleration on local field intensity. (x_0, y_0) is the coordinate of vehicle center position. θ is the angle between the speed direction and the connecting line, which connects a point and midpoint on the equal field intensity circle. Bring the water drop line model into (4) to obtain the kinetic energy field model shown in (6).

$$\left(\frac{|E_1| \cdot (x - x_0)}{-a/|a| \cdot e^{\varphi_1(v)}}\right)^2 + \left(\frac{|E_1| \cdot (y - y_0)}{sin(\theta/2)^{|a|} \cdot \kappa_2 \cdot e^{\varphi_1(v)}}\right)^2 = 1 \tag{6}$$

In addition, vehicle weight m and road environment factor γ are objective factors affecting the kinetic energy field intensity, and their influence degree will increase exponentially with the increase of vehicle weight and the deterioration of road conditions. Therefore, the relationship of the two is described as the product function $\varphi_2(\lambda, \gamma, m)$, which is expressed by (7).

$$\varphi_2(\lambda, \gamma, m) = \lambda \cdot \gamma \cdot m \tag{7}$$

When the function $\varphi_2(\lambda, \gamma, m)$ becomes larger and larger, the field intensity at the same position around the vehicle will become larger and larger. Therefore, it needs to be brought into the denominator of the elliptic equation. At this time, the kinetic energy field model can be expressed as:

$$\left(\frac{|E_1| \cdot (x - x_0)}{-a/|a| \cdot e^{\varphi_1(v)} \cdot \varphi_2(\lambda, \gamma, m)}\right)^2 + \left(\frac{|E_1| \cdot (y - y_0)}{sin(\theta/2)^{|a|} \cdot \kappa_2 \cdot e^{\varphi_1(v)} \cdot \varphi_2(\lambda, \gamma, m)}\right)^2 = 1 \tag{8}$$

The road condition factor γ is related to environmental visibility δ, pavement adhesion coefficient μ, road curvature ρ and slope τ [22]. With the decrease of environmental visibility and pavement adhesion coefficient, and the increase of road curvature and slope, the road condition factor will increase. So, the mathematical expression of road condition factor γ proposed by Wang is adopted by this paper [22], which is defined as:

$$\gamma = \gamma(\delta, \mu, \rho, \tau) = \left(\frac{\delta}{\delta^*}\right)^{\alpha_1} \left(\frac{\mu_i}{\mu^*}\right)^{\alpha_2} e^{(\rho - \rho^*)^{\alpha_3} + (\tau - \tau^*)^{\alpha_4}} \tag{9}$$

Among them, δ^* is the standard value of environmental visibility, μ^* is the standard value of pavement adhesion coefficient, ρ^* is the standard value of road curvature, τ^* is

the standard value of road slope, and $\alpha_1, \alpha_2, \alpha_3$ and α_4 are adjustment coefficients.

Finally, it should be noted that when the vehicle speed is zero or not zero, the influence of the vehicle on the front and rear is different. When the vehicle speed is not zero, the impact strength of the vehicle to the front shall be greater than that to the rear. Therefore, the density of the equal field intensity circle of kinetic energy field around the vehicle should be different. Multiple equal field circles must be moved in the direction of speed so that the elliptical focus of all equal field circles is at the center of the vehicle. Therefore, when the vehicle has speed, the scalar parameter equation of the kinetic energy field is shown in (10).

$$\begin{aligned}&\left(\frac{|E_1|\cdot(x-x_0)-(\sqrt{1-\kappa_2^2})\cdot e^{\varphi_1(v)}\cdot\varphi_2(\lambda,\gamma,m)}{-a/|a|\cdot e^{\varphi_1(v)}\cdot\varphi_2(\lambda,\gamma,m)}\right)^2\\&+\left(\frac{|E_1|\cdot(y-y_0)}{sin(\theta/2)^{|a|}\cdot\kappa_2\cdot e^{\varphi_1(v)}\cdot\varphi_2(\lambda,\gamma,m)}\right)^2\\&=1, v>0\end{aligned}\tag{10}$$

The field intensity direction at position (x, y) is:

$$\frac{\vec{r}}{|r|}=\frac{(x-x_0,y-y_0)}{\sqrt{(x-x_0)^2+(y-y_0)^2}}\tag{11}$$

In addition to the influence of the main body of the vehicle on rear-end collisions, drivers also play a crucial role in ensuring driving safety. When the vehicle is running, the driver needs to manipulate the vehicle, and the risk brought by the driver will exist. At this time, the driving risk field needs to superimpose a behavior field representing the driver factor [23]. When the vehicle stops, the driver does not need to operate the vehicle, so the risk it brings will disappear, and the driver behavior field does not need to be superimposed at this time. Essentially, the driver's behavior field is the result of the combined action of the driver factor and the vehicle kinetic energy field. So, the behavior field E_2 can be expressed as:

$$E_2=\beta\sigma E_1\tag{12}$$

β is adjustment coefficient. $\beta = 1$ means the vehicle is running, and $\beta = 0$ means the vehicle is stopped. Similarly, in Wang's paper, the driver factor σ is calculated by using driver's physiological & psychological factor $\sigma_{phy\&psy}$, cognitive factor $\sigma_{cognition}$, skill factor σ_{skill} and illegal factor σ_{laws} [22]. As shown in (13). We introduce this formula to calculate the driver factor σ. Its value range is (0,1). The higher the value, the greater the risk caused by the driver. Where η_1, η_2, η_3 and η_4 are adjustment coefficients.

$$\sigma=\eta_1\sigma_{phy\&psy}+\eta_2\sigma_{cognition}+\eta_3\sigma_{skill}+\eta_4\sigma_{laws}\tag{13}$$

To sum up, the driving risk field model E in this paper is:

$$E=E_1+E_2=E_1(1+\beta\sigma)\tag{14}$$

3) FIELD SHAPE ANALYSIS

In order to draw the shape of risk field under different combinations of speed and acceleration, the paper calibrated the model adjustment coefficients $\lambda, \kappa, \kappa_1$ and κ_2. First, the other dynamic parameters in the risk field model are assumed to be a set of fixed values $m = 2, \gamma = 1$ and $\sigma = 0.5$ to reduce the impact on subsequent calibration work. Then, on different magnitude ranges, we set the values for the four parameters. The four groups of parameters are combined freely. Under each group of parameters, the risk field shape maps of different speeds and accelerations are generated by MATLAB. Finally, considering that Wolf has proposed that the impact strength of the vehicle to the target 30 meters ahead and 2 meters to the side should be roughly the same [34]. Therefore, in order to coordinate the horizontal and vertical ratios of the risk field, the paper selects a set of relatively reasonable adjustment parameters $\lambda = 2, \kappa = 1, \kappa_1 = 0.2$ and $\kappa_2 = 0.4$ for the subsequent calculation. The risk field shape obtained by this group of parameters is drawn in Fig. 3. The black dot is the vehicle position.

As shown in Fig. 3 (a) (b) (c). It is obvious that when the vehicle is stationary, the equal field intensity circle is evenly distributed around the vehicle. However, when the vehicle has speed, the equal field intensity circle is obviously unevenly distributed. With the increase of speed, all equal field intensity circles are gradually sparse in front of the speed and gradually become dense in the rear of the speed, and the risk field shape becomes more and more wide and long. As shown in Fig. 3 (b). A coordinate system is established with the vehicle as the central point. The distance between the vehicle and the equal field intensity point gradually decreases from the front of the speed to the rear of the speed. The above shows that the risk field in this paper realizes the adjustment of speed to the transverse and longitudinal range of field intensity. Fig. 3 (d) (e) (f) also shows that the introduction of water drop line realizes the opposite weakening effect of acceleration and deceleration on local field intensity. In general, the change of driving risk field shape with speed, acceleration and deceleration are consistent with the original design idea.

B. CONSTRUCTION OF VEHICLE OPERATION INTERACTION RISK MODEL

1) VEHICLE OPERATION INFLUENCE FUNCTION

In a rear-end collision, in addition to the impact of the following vehicle on the leading vehicle, the operation state of the leading vehicle will also have an effect on the following vehicle. In the same way as the driving risk field, the paper describes the coupling function Q of the leading vehicle's operating parameters speed, weight, driver factor and road environment factor as the influence function of the leading vehicle on the rear-end collision. When the operating parameters of the leading vehicle are lower speed, heavier weight, more unstable driver and worse road environment, its risk impact on following vehicle will also be greater. But when the leading vehicle stops, the influence of its driver

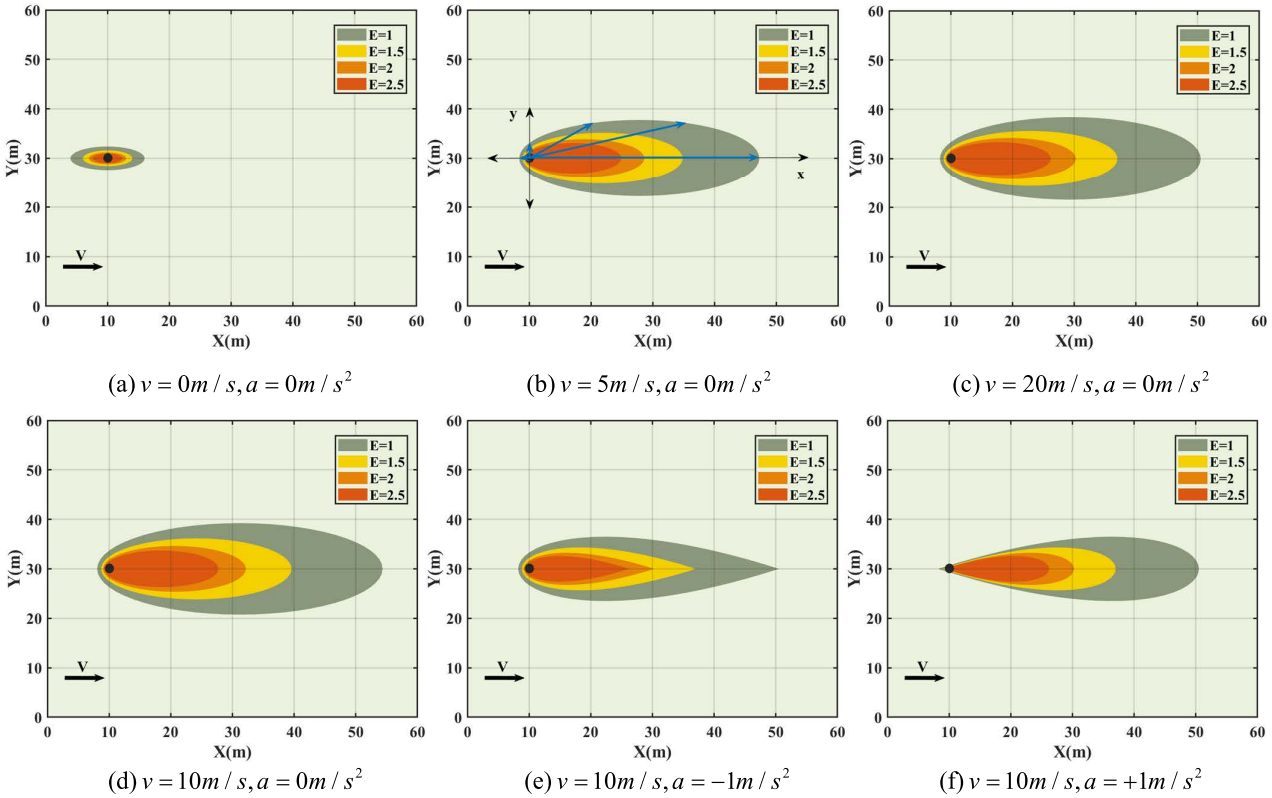

(a) $v = 0m/s, a = 0m/s^2$ (b) $v = 5m/s, a = 0m/s^2$ (c) $v = 20m/s, a = 0m/s^2$

(d) $v = 10m/s, a = 0m/s^2$ (e) $v = 10m/s, a = -1m/s^2$ (f) $v = 10m/s, a = +1m/s^2$

FIGURE 3. Driving risk field shape.

will disappear. Referring to the influence function expression of the paper [22], we introduce the parameter σ to adjust whether the influence of the driver exists, and obtains the operation influence function of the leading vehicle as shown in (15).

$$Q = \gamma \cdot m \cdot e^{-v^{\kappa_2}} \cdot (1 + \beta\sigma) \tag{15}$$

2) VEHICLE OPERATION INTERACTION RISK MODEL

The paper compares the risk field to the electric field, so the interaction between the following vehicle and the leading vehicle is like the relationship between the electric field and the electric charge. Based on this, we describe the operation interaction function value $F_{fo,le}(t)$ of the two vehicles as their risk field force. Then, according to the classical calculation formula of electric field force $F = Q \cdot E$, the risk field forces between two vehicles can be calculated by (16) and (17). The two forces $F^{ac}_{fo,le}(t)$ and $F^{sa}_{fo,le}(t)$ are the interaction results of the leading vehicle being in an accident state or a safety state, respectively.

$$F^{ac}_{fo,le}(t) = Q^{ac}_{le}(t) \cdot E_{fo}(t) \tag{16}$$

$$F^{sa}_{fo,le}(t) = Q^{sa}_{le}(t) \cdot E_{fo}(t) \tag{17}$$

Among them, $Q^{ac}_{le}(t)$ is the operation influence value of the leading vehicle in the accident state, and $Q^{sa}_{le}(t)$ is the operation influence value of the leading vehicle in the safety state.

Theoretically, the value range of risk field force is 0 to positive infinity, and the value range of risk probability is 0 to 1. In order to make the risk field force be able to express the vehicle operation interaction risk, the paper uses the hyperbolic tangent function to bring out the convert of risk field force. Fig. 4 is a partial image of this function. The setting of risk field model parameters can affect the magnitude of risk field force. This may lead to a large number of risk field force values concentrated in local interval, resulting in the corresponding risk probability values concentrated in a small interval. For example, if the risk field force of the paper experiment is generally less than 0.55 or generally greater than 0.55, the risk probability value will be concentrated in 0 to 0.5 or 0.5 to 1.0. In order to make the risk probability distribution between 0 and 1, the coefficient ω is introduced to adjust the range of risk field forces. Thus, the operation interaction risk model is shown in (18).

$$\phi(|F_{fo,le}(t)|) = \tanh(\omega|F_{fo,le}(t)|), |F_{fo,le}(t)| \in (0, +\infty), \quad 0 < \omega < 1 \tag{18}$$

The coefficient ω needs to be calibrated through a set of risk field force and risk probability. This paper defines these two values as critical risk field force F_c and critical risk probability ξ. It means that under the critical risk field force, the risk probability of vehicle interaction is the critical risk value to distinguish high-risk interaction from low-risk

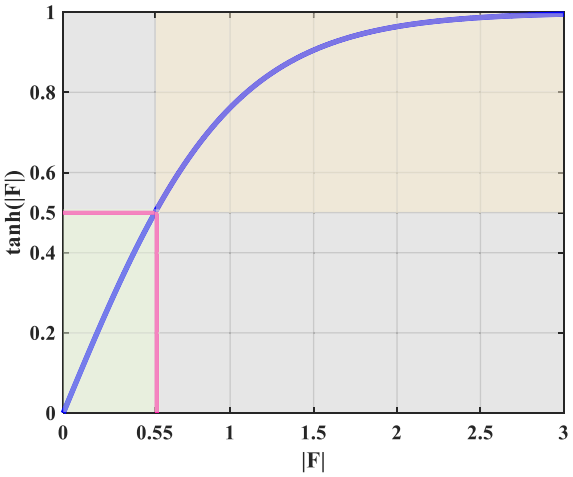

FIGURE 4. Hyperbolic tangent function diagram in the range of 0 to 3 positive variables.

interaction. Thus, the coefficient ω can be expressed as:

$$\omega = \frac{arc\tanh(\xi)}{|F_c|} \tag{19}$$

Finally, the vehicle operation interaction risk model is shown in (20). $\phi(|F_{fo,le}(t)|)$ is the operation interaction risk probability.

$$\phi(|F_{follow,lead}(t)|) = \tanh(\frac{arc\tanh(\xi)|F_{follow,lead}(t)|}{|F_c|}), \quad |F_{follow,lead}(t)| \in (0, +\infty) \tag{20}$$

C. CONSTRUCTION OF SECONDARY REAR-END COLLISION ACCIDENT RISK PROPAGATION MODEL

1) RISK PROPAGATION FRAMEWORK BASED ON DBN

This paper only studies the risk propagation characteristics of secondary rear-end collisions on single-lane roads, and uses dynamic Bayesian network to describe the propagation process of accident risk. Considering the vehicles on the single lane as the nodes of the dynamic Bayesian network, an accident risk propagation framework is established. As shown in Fig. 5. The framework can not only express the transfer process of the leading vehicle's risk to the following vehicle, but also express the operation interaction process of the two vehicles. In this way, through the probabilistic reasoning of the dynamic Bayesian network, the risk of the leading vehicle and the interaction risk of the two vehicles can be coupled to describe the rear-end collision risk of the following vehicle, so as to establish a secondary rear-end collision accident risk propagation model.

When the leading vehicle is in an uncertain operation state at time t, it has accident probability $D_{le}^{ac}(t)$ and safety probability $D_{le}^{sa}(t)$, and the sum of the two probabilities is 1. The interaction between the influence function of the leading vehicle in these two operation states and the risk field of the following vehicle will generate two risk field forces $F_{fo,le}^{ac}(t)$ and $F_{fo,le}^{sa}(t)$. Through the vehicle operation interaction risk model, the two forces can be transformed into the two vehicle interaction risks $\phi(|F_{fo,le}^{ac}(t)|)$ and $\phi(|F_{fo,le}^{sa}(t)|)$. Finally, by combining $D_{le}^{ac}(t)$, $D_{le}^{sa}(t)$, $\phi(|F_{fo,le}^{ac}(t)|)$ and $\phi(|F_{fo,le}^{sa}(t)|)$ with the total probability inference reasoning process of the dynamic Bayesian network, the accident probability $D_{fo}^{ac}(t)$ and safety probability $D_{fo}^{sa}(t)$ of the following vehicle can be calculated. The accident probability of the following vehicle is its rear-end risk. Finally, the secondary rear-end collision accident risk propagation model DBAR is obtained, as shown in (21).

$$DBAR_{fo}(t) = D_{fo}^{ac}(\mathrm{t})=D_{le}^{ac}(t)\cdot\phi(|F_{fo,le}^{ac}(t)|) + D_{le}^{sa}(t)\cdot\phi(|F_{fo,le}^{sa}(t)|) \tag{21}$$

2) ACCIDENT VEHICLE RISK MODEL

As the root node of the dynamic Bayesian network composed of continuous vehicles, the accident vehicle needs to first determine its risk probability at every moment in the probabilistic reasoning process of the risk propagation model. At the accident time $t = 0$, the accident vehicle happens to have an accident. At this time, its accident probability is $D_{accid}^{ac}(t = 0) = 1$ and the safety probability is $D_{accid}^{sa}(t = 0) = 0$. In the subsequent period $t \geq 1$, the operation state of the accident vehicle may change, so the accident probability $D_{accid}^{ac}(t \geq 1)$ and safety probability $D_{accid}^{sa}(t \geq 1)$ of the accident vehicle will also change accordingly. So, the paper designs the risk transfer probabilities during the disposal period for the accident vehicle. At this time, the risk probability of the accident vehicle can be expressed as:

$$D_{accid}^{ac}(t \geq 1) = D_{accid}^{ac}(t-1)\cdot p(d_{accid}^{ac}(t)/d_{accid}^{ac}(t-1)) + D_{accid}^{ac}(t-1)\cdot p(d_{accid}^{ac}(t)/d_{accid}^{sa}(t-1)) \tag{22}$$

$$D_{accid}^{sa}(t \geq 1) = 1 - D_{accid}^{ac}(t \geq 1) \tag{23}$$

$p(d_{accid}^{ac}(t)/d_{accid}^{ac}(t-1))$ is the probability that the accident vehicle is in the accident state at time t-1 and it is still in the accident state at time t. $p(d_{accid}^{ac}(t)/d_{accid}^{sa}(t-1))$ is the probability that the accident vehicle is in the safety state at time t-1 and it is in the accident state at time t.

3) SECONDARY REAR-END COLLISION ACCIDENT RISK PROPAGATION MODEL

It is assumed that the number of the following vehicle is 1 to N. Combined with accident vehicle risk model and vehicle operation interaction risk model, the specific calculation process of secondary rear-end collision accident risk propagation model is shown in (24) to (27).

Firstly, under the accident state of the leading vehicle, its speed is marked as zero, and under the safety state of the leading vehicle, its speed is the current value. So, its two

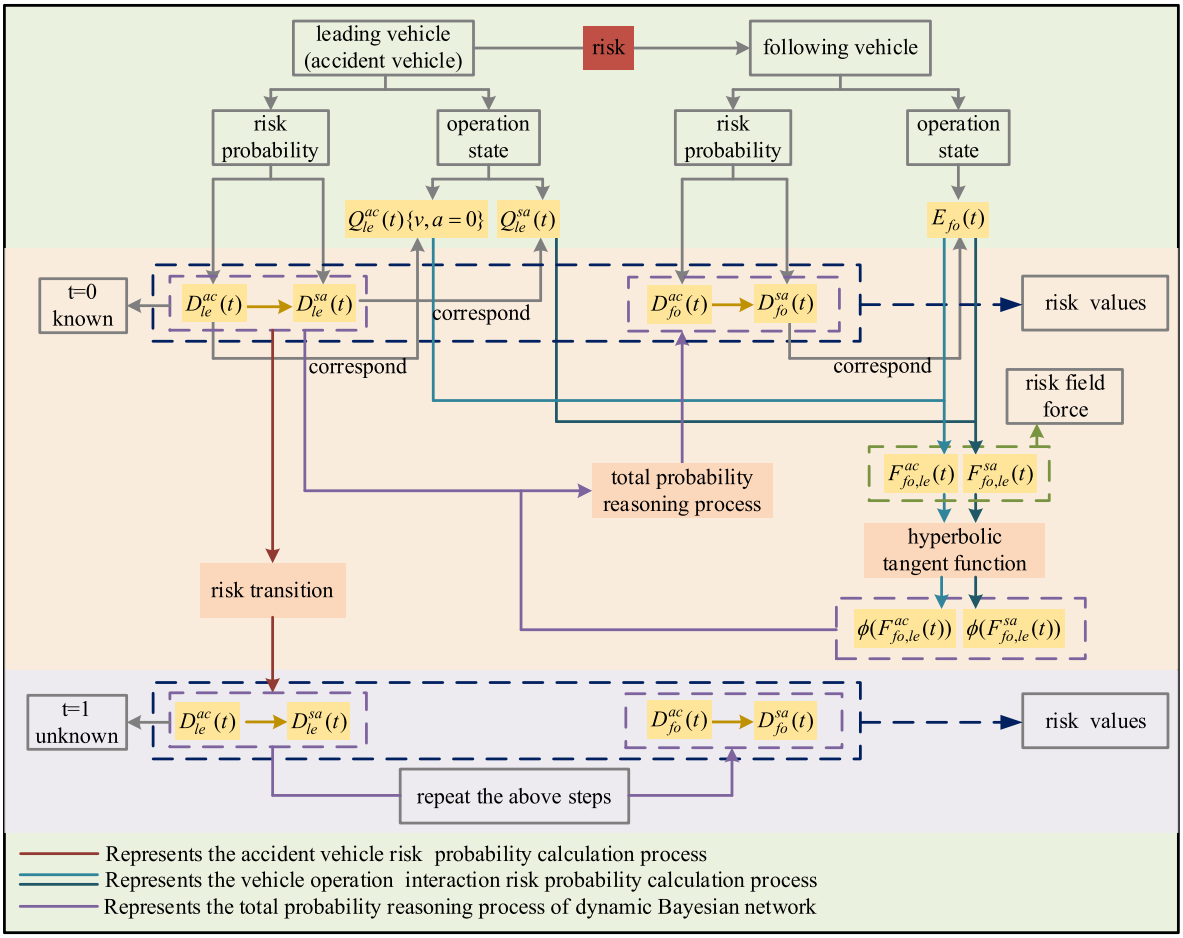

FIGURE 5. Single-lane road risk propagation framework.

influence function values can be calculated as:

$$Q_{le}^{ac}(t) = \gamma_{le}(t) \cdot m_{le}(t) \tag{24}$$

$$Q_{le}^{sa}(t) = \gamma_{le}(t) \cdot m_{le}(t) \cdot e^{-v_{le}(t)^{\kappa_2}}(1 + \beta_{le}(t)\sigma_{le}(t)) \tag{25}$$

Secondly, on single-lane road, the longitudinal distance between vehicles is zero. By simplifying (14), the risk field intensity value of the following vehicle can be expressed by (26).

$$E_{fo}(t) = \frac{\lambda \cdot \gamma_{fo}(t) \cdot m_{fo}(t) \cdot e^{(\kappa v_{fo}(t))^{\kappa_1}} \cdot (-\frac{a_{fo}(t)}{|a_{fo}(t)|} + \sqrt{1-\kappa_2^2})}{|(x_{le}(t) - x_{fo}(t))|} \times (1 + \beta_{fo}(t)\sigma_{fo}(t)) \tag{26}$$

Thus, according to (16) and (17), the risk field forces $F_{fo,le}^{ac}(t)$ and $F_{fo,le}^{sa}(t)$ between two vehicles can be solved respectively. Then, according to (20), the operation interaction risks corresponding to the two forces can be solved.

Finally, accident vehicle risk and vehicle operation interaction risk are brought into (21) to obtain the final secondary rear-end collision accident risk propagation model DBAR. As shown in (27).

$$DBAR_{fo}(t) = \begin{cases} 1 \cdot \tanh(\dfrac{arc\tanh(\xi)|F_{fo,le}^{ac}(t)|}{|F_c|}) \\ +0 \cdot \tanh(\dfrac{arc\tanh(\xi)|F_{fo,le}^{sa}(t)|}{|F_c|}), & fo = 1 \\ D_{le}^{ac}(t) \cdot \tanh(\dfrac{arc\tanh(\xi)|F_{fo,le}^{ac}(t)|}{|F_c|}) \\ +D_{le}^{sa}(t) \cdot \tanh(\dfrac{arc\tanh(\xi)|F_{fo,le}^{sa}(t)|}{|F_c|}), & 2 \le fo \le N \end{cases} \tag{27}$$

IV. EXPERIMENTAL ANALYSIS

This section will use the simulation data to calculate the vehicle rear-end collision risk, and carry out relevant experimental analysis. The main contents include experimental scenario construction, model parameter calibration, rationality test of risk propagation model and analysis of the risk propagation characteristics of rear-end collision accidents.

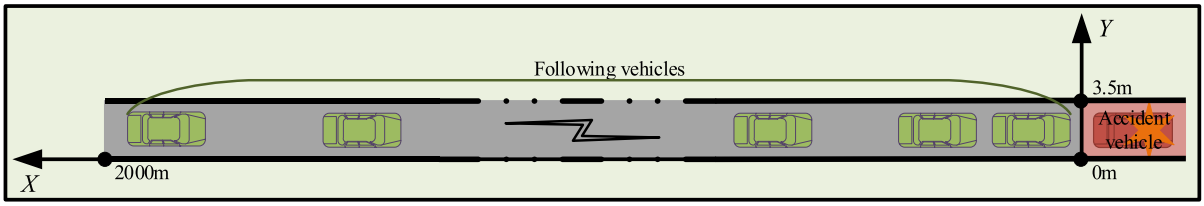

FIGURE 6. Experimental scenario.

A. CONSTRUSTION OF EXPERIMENTAL SCENARIO

The experimental scenario is shown in Fig. 6. Single-lane road has been closed due to traffic accident. Following vehicles can only stop and wait. The experimental road is 2000 meters long, the lane is 3.75 meters wide, the safe parking distance is 5 meters, and the accident vehicle is located at 0 meters of the road. The experiment uses VISSIM to simulate vehicle operation, and collects the speed, acceleration, weight, and position coordinate data of all vehicles. The observation time is 20 minutes. The time granularity of data acquisition is 1s. In addition, due to the limitation of simulation software, some model parameters cannot be modified and collected. Therefore, in all experiments, we assumed the road condition factor γ as the ideal value 1 and the driver factor σ as the equilibrium value 0.5. Then, take these values as the standard for model calculation. They will not affect the experimental conclusion. The parameters required for the experiment are shown in Table 1.

B. CALIBRATION OF MODEL PARAMETERS

1) RISK TRANSFER PROBABILITY CALIBRATION

Rear-end accident risk propagation starts from the accident vehicle. The risk probability of the accident vehicle at time $t = 0$ has been determined. Next, we calculate the risk probability of the accident vehicle at each moment after the accident. In the simulation experiment, the accident vehicle has been in the disposal period. Since the operation state of the accident vehicle existing in the lane is unchanged during the disposal period, its influence on the following vehicle is also unchanged. So, the paper considers that the accident probability and safety probability of the accident vehicle during the accident disposal are consistent with the probabilities at time $t = 0$. Thus, the risk transfer probability of the accident vehicle at each moment during the accident disposal period is calibrated as $p(d^{ac}_{accid}(t)/d^{ac}_{accid}(t-1)) = 1$ and $p(d^{ac}_{accid}(t)/d^{sa}_{accid}(t-1)) = 0$.

2) CRITICAL RISK PROBABILITY CALIBRATION

We have defined the critical risk probability as the critical risk value that distinguishes high-risk and low-risk interactions of vehicles. In the value range of risk probability, 0.5 is the intermediate value. Usually in people's wide cognition, the median value is generally used as the dividing line to distinguish size, length or other measures. The paper also adopts this idea, arguing that if the risk probability is higher than 0.5, it is high-risk vehicle interaction, and if the risk probability is lower than 0.5, it is low-risk vehicle interaction. Thus, the critical risk probability is calibrated as 0.5.

3) CRITICAL RISK FIELD FORCE CALIBRATION

When the parameters of the risk field model are different, the magnitude of the risk field force is also quite different. Therefore, in order to determine the critical risk field force under the parameters of the paper, we statistically analyze the cumulative distribution characteristics of numerous risk field forces to find the most reasonable force value. A large number of experiments are needed to collect the risk field force. In order to input reasonable traffic flow parameters into the simulation model and conduct rich experiments, eleven traffic states are selected according to the Greenshields model, which are S1(400,74.0), S2(800,70.3), S3(1200,66.1), S4(1600,61.0), S5(2000,54.5), S6(2400,38.7), S7(2000,22.9), S8(1600,16.4), S9(1200,11.3), S10(800,7.1) and S11(400,3.4). They involve peak period, middle peak period and low peak period in traffic operation. As shown in Fig. 7. One experiment is carried out for each traffic state, and all risk field force values for each experiment are calculated.

Fig. 8 shows the cumulative distribution curve of all risk field forces. The ten quantiles of the curve are uniformly selected to calculate the corresponding risk field force, slope and slope difference. As shown in Table 2. At the 45% quantile, the slope difference of the curve becomes negative. It shows that the cumulative rate of risk field force began to decrease. But, the slope of the curve is still very large, and the accumulation rate of risk field force is still very fast. Until the 85% quantile, the slope of the curve decreases significantly and the slope becomes very small. This shows that the number of large risk field forces began to decrease significantly. In practice, the number of high-risk vehicle interactions should be significantly less than that of low-risk vehicle interactions. Based on this, the paper takes the risk field force value of the 85% quantile of the curve as the critical risk field force. Then $|F_c|$ is calibrated as 0.93. Our calibration principle is consistent with the actual situation.

C. RISK PROPAGATION MODEL TEST

In order to prove the rationality of the secondary rear-end collision risk propagation model DBAR, it is compared with three methods. The FR method is a risk field risk assessment

TABLE 1. Parameters required for the experiment.

Parameter	Symbol	Parameter	Symbol
speed	v	position coordinate	(x, y)
acceleration	a	road condition factor	γ
weight	m	driver factor	σ

TABLE 2. Parameter value corresponding to the quantile on the curve.

Quantile	5%	15%	25%	35%	45%	55%	65%	75%	85%	95%
Risk field force	0.26	0.35	0.41	0.47	0.52	0.58	0.68	0.79	0.93	1.45
Slope	1.11	1.67	1.67	2.00	**1.67**	1.00	0.91	0.71	**0.19**	0.15
Slope difference	1.11	0.56	0.00	0.33	**-0.33**	-0.67	-0.09	-0.20	**-0.52**	-0.04

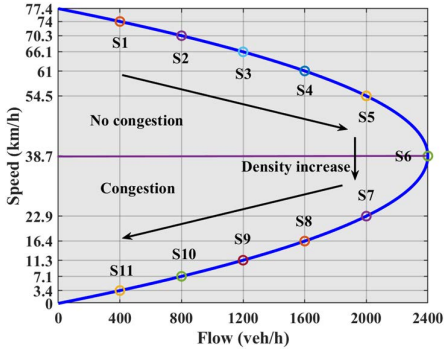

FIGURE 7. Traffic state points on Greenshields model curve.

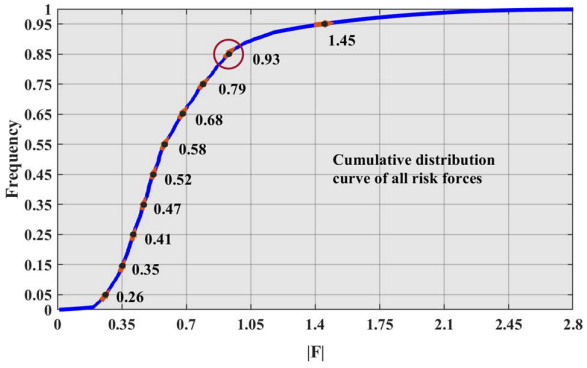

FIGURE 8. Cumulative distribution curve of risk field forces.

method that does not consider the risk transfer of the leading vehicle, and the rear-end collision risk calculated by it can be expressed as $FR_{fo}(t) = \phi(|F^{sa}_{fo,le}(t)|)$. The TTC method is a classic conflict index risk assessment method, which is widely used and suitable for our simulation scenarios. Its assessed rear-end risk is denoted as $1/TTC$. The PFI method is the potential field index method, which risk field mainly emphasizes the impact of acceleration on the field intensity [26].

We randomly collect a group of operation data of the leading & following vehicle from each experiment. The sampling time is from 8 seconds (− 8s) before the leading vehicle stops to 1 second (+ 1s) after the leading vehicle stops. A total of ten moments. Then, use the DBAR, FR, TTC and PFI methods to calculate the rear-end collision accident risk of the following vehicle, and draw the risk evolution curves. Fig. 9 is the result of partial experiments. The horizontal axis is the ten moments before and after the leading vehicle stops.

Obviously, TTC curve in each experiment is discontinuous, and its value sometimes becomes zero and sometimes increases. This result is not conducive to assessing the evolution trend of the following vehicle risk. What's more. In each experiment, when TTC value is zero, the speed of the following vehicle is not zero and the distance between the two vehicles is very small. In this case, the following vehicle risk should not be zero. So, TTC result deviates from the actual situation. In contrast, the curves of DBAR, FR and PFI are smooth and continuous, which can describe the evolution trend of rear-end collision risk. This is also the advantage of using driving risk field for risk assessment.

However, the PFI curve often shows the phenomenon that the risk increases suddenly and then decreases. This may be related to the sudden change of the acceleration of the leading vehicle. When the leading vehicle decelerates, the following vehicle risk will increase. This is the advantage of PFI. However, during the braking process of the leading vehicle, the following risk should be directly related to the speed of the two vehicles and the following distance. As the following vehicle speed is gradually greater than the leading vehicle and the following distance is gradually reduced, the following vehicle risk will gradually increase. But PFI weakens their influence. In contrast, DBAR can better describe this process.

In addition, all pictures show that when the leading vehicle stops, the risk assessment results of DBAR and FR are consistent. And in the two experiments of S1 and S9, the curves between − 8s and − 3s coincide relatively. After inspection, during this period, the leading vehicle risks in

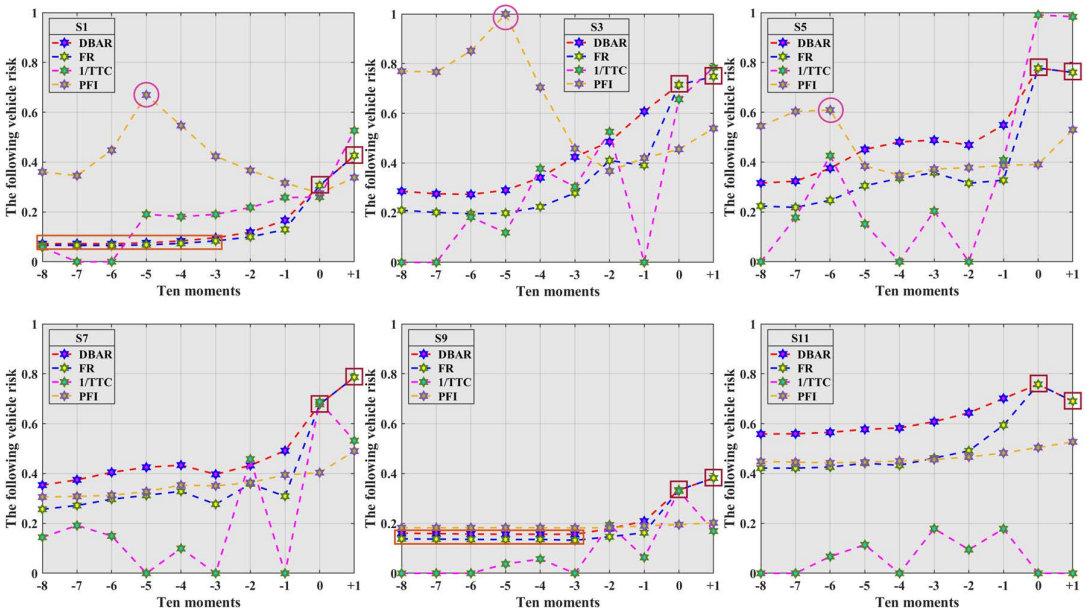

FIGURE 9. Evolution curve of the following vehicle risk.

these two experiments are very small, close to zero. So, the above analysis shows that when the leading vehicle is in a deterministic risk state, such as safe driving and parking, there is no difference in the risk assessment results whether the risk state of the leading vehicle is considered or not.

However, the advantage of DBAR is that when the leading vehicle is in an uncertain risk state, its risk assessment result for the following vehicle is more accurate. For example, in all the pictures, there are many moments when the curves of DBAR and FR do not coincide. The risk values calculated by DBAR is usually greater than that of FR. At these moments, we calculated risk values of leading vehicles according to the average of DBAR and FR results. It is found that these risk values are relatively large, about 0.6-0.7. Usually, the more dangerous the leading vehicle is, the more dangerous the following vehicle will be affected by it. Therefore, this increased risk phenomenon just shows that DBAR realizes the potential accident risk perception of the following vehicle to the leading vehicle.

D. ANALYSIS OF RISK PROPAGATION CHARACTERISTICS

1) RISK MICRO PROPAGATION ANALYSIS

After the accident, the rear-end collision risk acts on the vehicle, which will cause the fluctuation of the vehicle risk. It belongs to the risk propagation at the micro level. Since different traffic states correspond to different vehicle operation states, this paper firstly studies the risk micro propagation characteristics under different traffic states [35], [36]. We analyze and compare the experimental results of eleven traffic states. Each experiments calculated the risk values of all vehicles within 20 minutes. And draw the risk evolution curve of ten following vehicles from the moment of accident ($t = 0$) to the moment after accident ($t = 8$). In order to reduce the page size occupied by the picture, we only show the experimental results of six traffic states for analysis and explanation.

Fig. 10 shows the micro propagation process of rear-end collision risk. The pink dotted line is the line where each vehicle's risk begins to be affected. The steeper the pink dotted line indicates the faster the risk micro spread. It can be seen that with the increase of traffic flow first and then decrease, the propagation speed of accident risk also shows the same law. This phenomenon shows that with the gradual increase of traffic flow, the micro propagation speed of risk also increases gradually. And the green dotted line is the line where each vehicle's risk end is affected. The lateral distance between the two lines represents the affected time of the vehicle risk. Obviously, under the high traffic flow state, the later the vehicle arrives, the longer its risk is affected. However, under the low traffic flow state, this phenomenon is not obvious.

Fig. 11 shows the risk mutation of ten following vehicles after the accident. By comparing the pictures, it can be seen that the risk mutation of the vehicle is more severe in the high-speed traffic state, and more gentle in the low-speed traffic state. And secondary accidents involving 4 vehicles, 3 vehicles and 1 vehicle occurred under the states of S2, S3 and S5, while no secondary accidents occurred under the states of S7, S8 and S10. Through this experimental result, we can roughly draw such a conclusion. When traffic state is the high-speed state, once there is an accident on the road, the following vehicles may have secondary accidents. And the faster the traffic speed, the more vehicles will have secondary accidents. Moreover, it can also be approximately considered that the S6 traffic state is the limit for judging whether a secondary rear-end collision accident occurs.

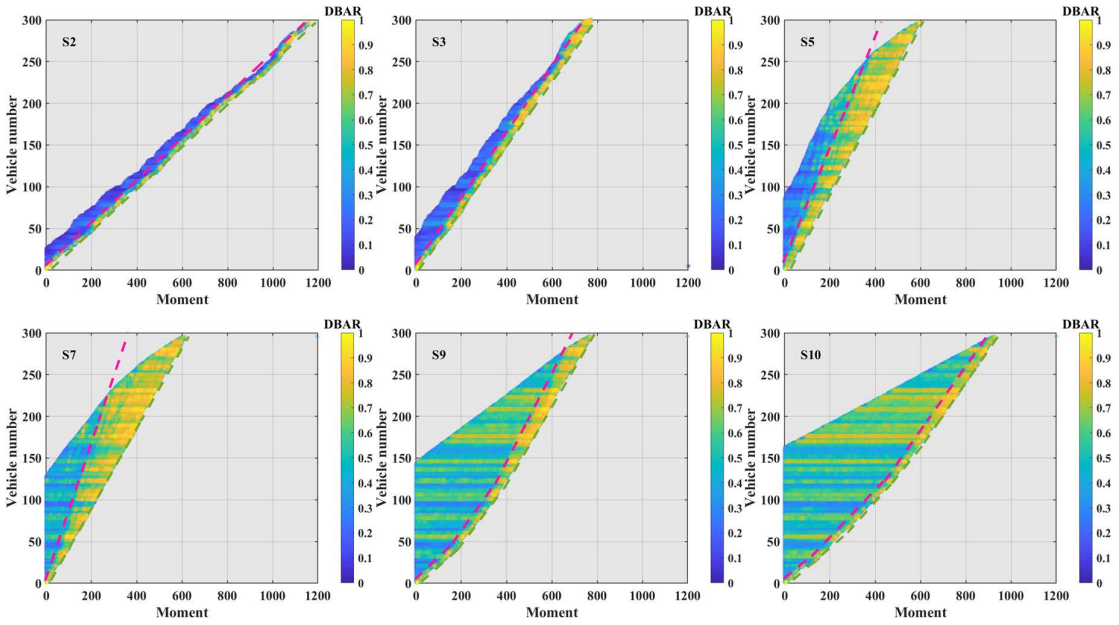

FIGURE 10. Risk micro propagation diagram.

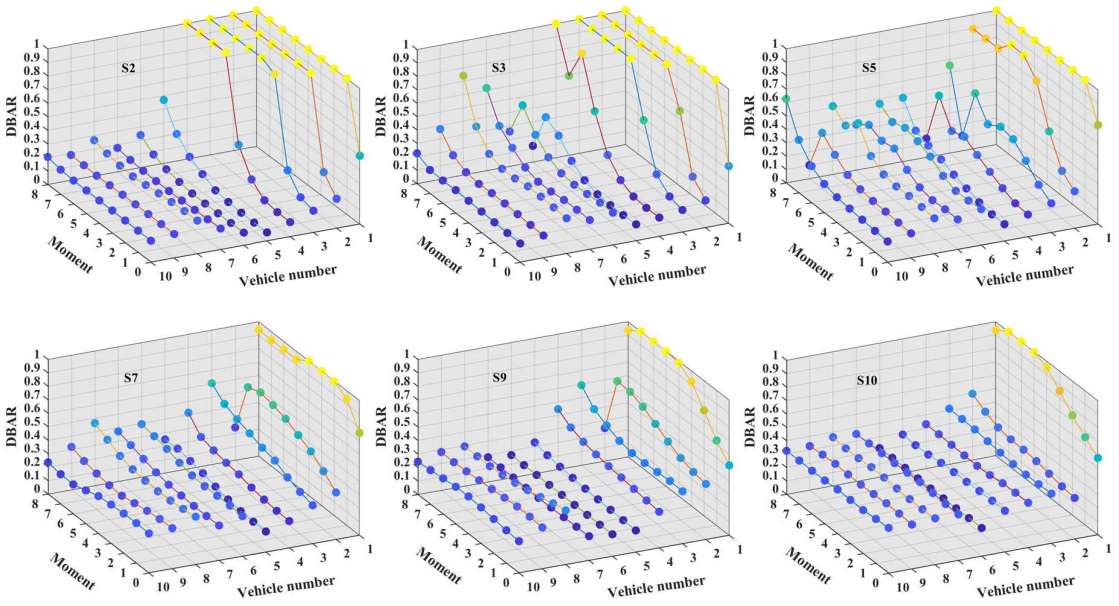

FIGURE 11. Risk increment diagram of following vehicles.

2) RISK MACRO PROPAGATION ANALYSIS

The road is the carrier of vehicles, so the vehicle risk can be mapped to the road risk at the vehicle location. The research on the risk micro propagation characteristics has shown that it has a certain change law with the change of traffic state. Next, the paper analyzes the risk macro propagation characteristics on the basis of the above. The observation time is discretized into 20 periods $T(T_1, T_2, \cdots, T_{20})$ in the unit of 1 minute, and the experimental road is discretized into 10 sections. $L(L_1, L_2, \cdots, L_{10})$ in the unit of 200 m. The paper counts the vehicle risk value in each period and section. The statistical results are shown in Fig. 12 and Fig. 13.

Fig. 12 is the scatter diagram of risk statistical results in this spatiotemporal discrete road. The red box indicates the risk distribution of each section when its risk is not affected. The position of the red box on the z-axis shows that when the traffic density gradually increases, the risk distribution range of each section gradually expands, the minimum risk value gradually increases, and the overall risk shows an upward trend.

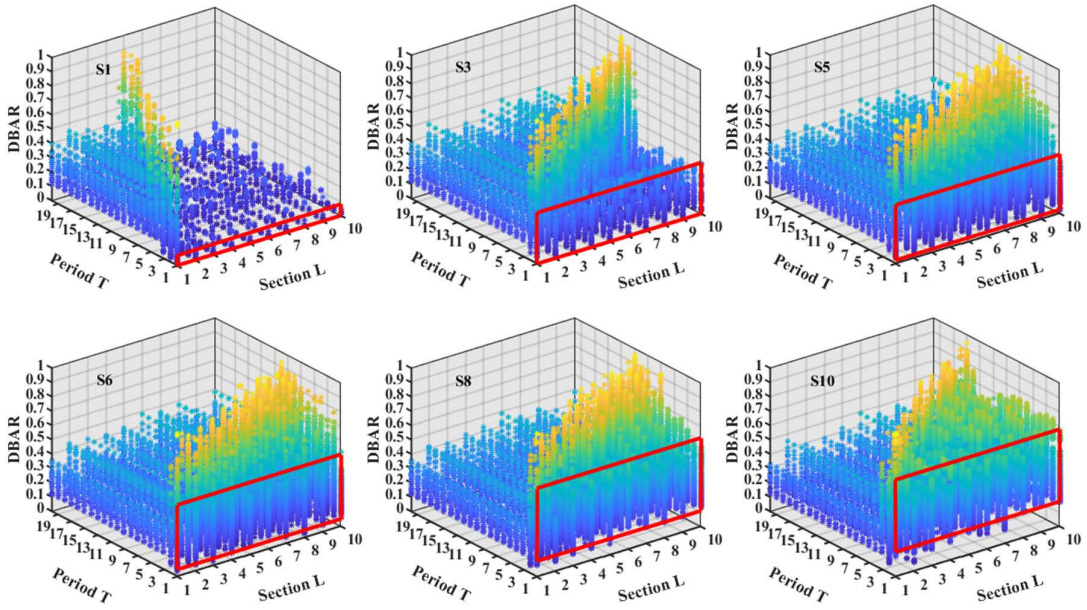

FIGURE 12. Scatter diagram of risk statistical results in spatiotemporal discrete road.

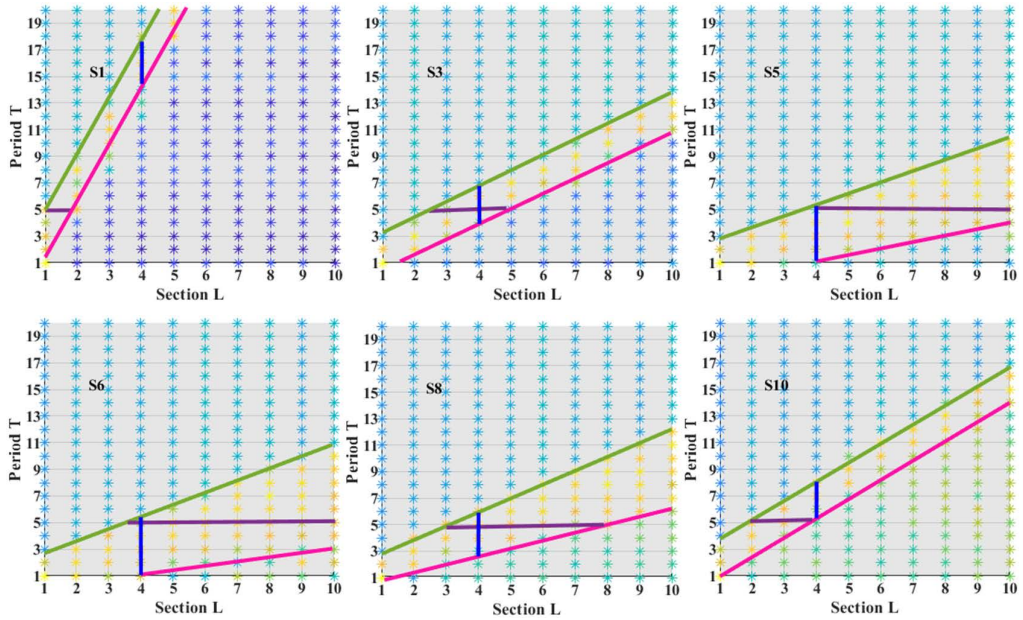

FIGURE 13. Risk macro propagation diagram.

Fig. 13 is a top view of Fig. 12. This figure can clearly express the spatiotemporal relationship of risk macro spread. The pink and green solid lines are the lines where each section risk begins to be affected and ends to be affected, respectively. Obviously, whether it is risk micro propagation or risk macro propagation, with the change of traffic state, the variation law of risk propagation speed in time and space is roughly the same. At the maximum flow traffic state of the Greenshields model curve, the risk propagation speed is the fastest. When transiting to S1 and S10 traffic states along the curve, the propagation speed will gradually slow down.

The blue solid line represents the impacted time of the risk on the fifth section. Its length shows that as the traffic flow increases, the affected time of risks on each section will be longer and longer, especially the section far from the accident location. And the purple solid line represents the affected range of the risk in the fifth period. Its length shows that as the traffic flow increases, the affected range of risks in each period will be larger and larger.

V. CONCLUSION

Accurate & real-time risk assessment and micro & macro risk propagation characteristics are of great significance for the prevention and control of secondary rear-end collision accidents. Therefore, this paper proposed a secondary rear-end collision accident risk assessment method to analyze the propagation characteristics of risk. Its advantage is that the risk assessment not only considers the operation state of the leading & following vehicle, but also considers the risk of the leading vehicle.

Firstly, we constructed a driving risk field suitable for rear-end collision scenarios with speed as the main factor, and proposed a vehicle operation influence function with the vehicle's own attributes as parameters. The two respectively express the operation state of the leading and following vehicles. Then, with the risk field force of the interaction between the two vehicles as the parameter, we constructed the vehicle operation interaction risk model. Finally, we proposed a rear-end collision risk propagation framework based on dynamic Bayesian network, and constructed a secondary rear-end accident risk propagation model through its total probability reasoning process.

According to the simulation data, we carried out a series of experimental analysis. (1) Through the cumulative distribution characteristics of numerous risk field forces, the critical risk field force is calibrated as 0.93. (2) By comparing with the methods TTC, FR and PFI, it is proved that DBAR method can describe risk evolution more continuously and accurately. (3) It is concluded that after the accident, with the increase of traffic flow, the micro and macro propagation speed of risk will accelerate, and the affected time of risks on each section and the affected range of risks in each period will increase; and with the increase of traffic speed, the number of vehicles that may have secondary accidents will gradually increase.

Our research only involves single lane accident scenarios. In the future, we can expand to multi-lane scenarios to adapt to more complex traffic networks.

REFERENCES

[1] J. Kim and D. Kum, "Collision risk assessment algorithm via lane-based probabilistic motion prediction of surrounding vehicles," *IEEE Trans. Intell. Transp. Syst.*, vol. 19, no. 9, pp. 2965–2976, Sep. 2018.

[2] G. F. Li, Y. Yang, T. Zhang, X. Qu, D. Cao, and B. Cheng, "Risk assessment based collision avoidance decision-making for autonomous vehicles in multi-scenarios," *Transp. Res. C, Emerg. Technol.*, vol. 122, Jan. 2021, Art. no. 102820.

[3] Y. Wu, M. Abdel-Aty, Q. Cai, J. Lee, and J. Park, "Developing an algorithm to assess the rear-end collision risk under fog conditions using real-time data," *Transp. Res. C, Emerg. Technol.*, vol. 87, pp. 11–25, Feb. 2018.

[4] Y. Y. Guo, T. Sayed, and M. Essa, "Real-time conflict-based Bayesian Tobit models for safety evaluation of signalized intersections," *Accident Anal. Prevention*, vol. 144, Sep. 2020, Art. no. 105660.

[5] L. Dimitriou, K. Stylianou, and M. A. Abdel-Aty, "Assessing rear-end crash potential in urban locations based on vehicle-by-vehicle interactions, geometric characteristics and operational conditions," *Accident Anal. Prevention*, vol. 118, pp. 221–235, Mar. 2018.

[6] C. Y. Fu and T. Sayed, "Comparison of threshold determination methods for the deceleration rate to avoid a crash (DRAC)-based crash estimation," *Accident Anal. Prevention*, vol. 153, Apr. 2021, Art. no. 106051.

[7] L. Zheng and T. Sayed, "From univariate to bivariate extreme value models: Approaches to integrate traffic conflict indicators for crash estimation," *Transp. Res. C, Emerg. Technol.*, vol. 103, pp. 211–225, Jun. 2019.

[8] C. Katrakazas, A. Theofilatos, M. A. Islam, E. Papadimitriou, L. Dimitriou, and C. Antoniou, "Prediction of rear-end conflict frequency using multiple-location traffic parameters," *Accident Anal. Prevention*, vol. 152, Mar. 2021, Art. no. 106007.

[9] Y. L. Ma and J. Y. Zhu, "Left-turn conflict identification at signal intersections based on vehicle trajectory reconstruction under real-time communication conditions," *Accident Anal. Prevention*, vol. 150, Feb. 2021, Art. no. 105933.

[10] K. Xie, K. Ozbay, H. Yang, and C. Li, "Mining automatically extracted vehicle trajectory data for proactive safety analytics," *Transp. Res. C, Emerg. Technol.*, vol. 106, pp. 61–72, Sep. 2019.

[11] J. Wang, Y. Zheng, X. Li, C. Yu, K. Kodaka, and K. Li, "Driving risk assessment using near-crash database through data mining of tree-based model," *Accident Anal. Prevention*, vol. 84, pp. 54–64, Nov. 2015.

[12] H. Y. Hu, Q. Wang, M. Cheng, and Z. H. Gao, "Cost-sensitive semi-supervised deep learning to assess driving risk by application of naturalistic vehicle trajectories," *Expert Syst. Appl.*, vol. 178, Sep. 2021, Art. no. 115041.

[13] F. M. Costela and J. J. Castro-Torres, "Risk prediction model using eye movements during simulated driving with logistic regressions and neural networks," *Transp. Res. F, Traffic Psychol. Behav.*, vol. 74, pp. 511–521, Oct. 2020.

[14] T. Chen, X. Shi, and Y. D. Wong, "Key feature selection and risk prediction for lane-changing behaviors based on vehicles' trajectory data," *Accident Anal. Prevention*, vol. 129, pp. 156–169, Aug. 2019.

[15] X. Shi, Y. D. Wong, M. Z.-F. Li, C. Palanisamy, and C. Chai, "A feature learning approach based on XGBoost for driving assessment and risk prediction," *Accident Anal. Prevention*, vol. 129, pp. 170–179, Aug. 2019.

[16] S. Kolekar, J. de Winter, and D. Abbink, "Human-like driving behaviour emerges from a risk-based driver model," *Nature Commun.*, vol. 11, no. 1, p. 13, Sep. 2020.

[17] F. A. Mullakkal-Babu, M. Wang, H. Farah, B. van Arem, and R. Happee, "Comparative assessment of safety indicators for vehicle trajectories on highways," *Transp. Res. Rec., J. Transp. Res. Board*, vol. 2659, no. 1, pp. 127–136, Jan. 2017.

[18] Y. L. Ma, L. Y. Fan, T. L. Lü, and L. Guo, "Quantification classification method for driving risk quantization using Bayesian network," *Ha'erbin Gong ye da Xue Xue Bao*, vol. 52, no. 3, pp. 33–37, 2020.

[19] Y. Ma, S. Qi, L. Fan, W. Lu, C.-Y. Chan, and Y. Zhang, "Dynamic Bayesian network approach to evaluate vehicle driving risk based on on-road experiment driving data," *IEEE Access*, vol. 7, pp. 135050–135062, 2019.

[20] L. Yan, Z. Huang, Y. Zhang, L. Zhang, D. Zhu, and B. Ran, "Driving risk status prediction using Bayesian networks and logistic regression," *IET Intell. Transport Syst.*, vol. 11, no. 7, pp. 431–439, Sep. 2017.

[21] N. Ding, S. Cui, C. Zhao, Y. Wang, and B. Chen, "Multi-link scheduling algorithm of LLC protocol in heterogeneous vehicle networks based on environment and vehicle-risk-field model," *IEEE Access*, vol. 8, pp. 224211–224223, 2020.

[22] J. Q. Wang, J. Wu, and Y. Li, "The driving safety field based on driver–vehicle–road interactions," *IEEE Trans. Intell. Transp. Syst.*, vol. 16, no. 4, pp. 2203–2214, Aug. 2015.

[23] J. Q. Wang, J. Wu, and Y. Li, "Concept, principle and modeling of driving risk field based on driver-vehicle-road interaction," *China J. Highway Transp.*, vol. 29, no. 1, pp. 105–114, 2016. [Online]. Available: https://go.exlibris.link/3D9wwKBS

[24] J. Q. Wang, H. Y. Huang, Y. Li, H. C. Zhou, J. X. Liu, and Q. Xu, "Driving risk assessment based on naturalistic driving study and driver attitude questionnaire analysis," *Accident Anal. Prevention*, vol. 145, Sep. 2020, Art. no. 105680.

[25] J. Wang, J. Wu, X. Zheng, D. Ni, and K. Li, "Driving safety field theory modeling and its application in pre-collision warning system," *Transp. Res. C, Emerg. Technol.*, vol. 72, pp. 306–324, Nov. 2016.

[26] L. H. Li, J. Gan, Z. W. Yi, X. Qu, and B. Ran, "Risk perception and the warning strategy based on safety potential field theory," *Accident Anal. Prevention*, vol. 148, Dec. 2020, Art. no. 105805.

[27] L. H. Li, J. Gan, X. Qu, W. Q. Lu, P. P. Mao, and B. Ran, "A dynamic control method for cavs platoon based on the MPC framework and safety potential field model," *KSCE J. Civil Eng.*, vol. 25, no. 5, pp. 1874–1886, May 2021.

[28] L. H. Li, J. Gan, K. Zhou, X. Qu, and B. Ran, "A novel lane-changing model of connected and automated vehicles: Using the safety potential field theory," *Phys. A, Stat. Mech. Appl.*, vol. 559, Dec. 2020, Art. no. 125039.
[29] L. Li, J. Gan, X. Ji, X. Qu, and B. Ran, "Dynamic driving risk potential field model under the connected and automated vehicles environment and its application in car-following modeling," *IEEE Trans. Intell. Transp. Syst.*, vol. 23, no. 1, pp. 122–141, Jan. 2022.
[30] F. A. Mullakkal-Babu, M. Wang, X. L. He, B. van Arem, and R. Happee, "Probabilistic field approach for motorway driving risk assessment," *Transp. Res. C, Emerg. Technol.*, vol. 118, Sep. 2020, Art. no. 102716.
[31] H. Huang, J. Wang, C. Fei, X. Zheng, Y. Yang, J. Liu, X. Wu, and Q. Xu, "A probabilistic risk assessment framework considering lane-changing behavior interaction," *Sci. China Inf. Sci.*, vol. 63, no. 9, p. 15, Aug. 2020.
[32] J. Kim, A. U. A. Shah, and H. G. Kang, "Dynamic risk assessment with Bayesian network and clustering analysis," *Rel. Eng. Syst. Saf.*, vol. 201, Sep. 2020, Art. no. 106959.
[33] C. Katrakazas, M. Quddus, and W.-H. Chen, "A new integrated collision risk assessment methodology for autonomous vehicles," *Accident Anal. Prevention*, vol. 127, pp. 61–79, Jun. 2019.
[34] M. T. Wolf and J. W. Burdick, "Artificial potential functions for highway driving with collision avoidance," in *Proc. IEEE Int. Conf. Robot. Autom.*, New York, NY, USA, May 2008, pp. 3731–3736, doi: 10.1109/robot.2008.4543783.
[35] T. Liu, Z. B. Li, P. Liu, C. C. Xu, and D. A. Noyce, "Using empirical traffic trajectory data for crash risk evaluation under three-phase traffic theory framework," *Accident Anal. Prevention*, vol. 157, Jul. 2021, Art. no. 106191.
[36] X. Wang, Z. W. Qu, X. M. Song, Q. W. Bai, Z. T. Pan, and H. T. Li, "Incorporating accident liability into crash risk analysis: A multidimensional risk source approach," *Accident Anal. Prevention*, vol. 153, Apr. 2021, Art. no. 106035.

XIANMIN SONG received the B.S. and Ph.D. degrees in traffic engineering from Jilin University, Changchun, China, in 2005 and 2008, respectively. She is currently a Professor with the School of Transportation, Jilin University. Her research interests include intelligent traffic control, traffic flow theory, and traffic big data.

YAQIAN SUN received the B.S. degree in traffic engineering from Jilin University, Changchun, China, in 2019, where she is currently pursuing the master's degree with the School of Transportation. Her research interests include traffic accident risk assessment and vehicle conflict analysis.

PENGFEI TAO received the B.S. degree in computer science and technology and the M.S. and Ph.D. degrees in traffic engineering from Jilin University, China. He is currently an Associate Professor with the School of Transportation, Jilin University. His research interests include driving behavior analysis and autonomous vehicles.